


 CrossMark
click for updates

 Cite this: *Lab Chip*, 2015, 15, 1445

 Received 11th December 2014,
Accepted 5th January 2015

DOI: 10.1039/c4lc01451k

www.rsc.org/loc

A convection-driven long-range linear gradient generator with dynamic control†

 Hao Wang,^a Chia-Hung Chen,^{*b} Zhuolin Xiang,^a Ming Wang^b and Chengkuo Lee^{*a}

We developed a novel gradient generator to achieve long range and linear chemical gradients with a dynamic control function. The length of the gradient can be on the centimetre scale. The gradient profile can be tuned by changing the flow rates. The device can work in both high flow rate regimes with large shear stress and low flow rate regimes with minimum shear stress. The drug screening function was demonstrated by the viability test of PC-9 cancer cells.

Introduction

Nowadays, engineering various gradients has attracted extensive attention for biomedical applications because gradients play essential roles in many biological activities and regulate a number of cellular functions *in vivo*. Chemical gradients have been shown to affect various cell behaviours, such as migration, proliferation, and differentiation during development.^{1,2} Microfluidic devices offer the possibility of generating complex and well defined gradient profiles.

One of the most popular methods for generating chemical gradients is to leverage the Christmas tree design.^{3–20} Two or more fluids are mixed in different ratios by a channel network, forming a gradient in the main channel by laminar flow. Because of the laminar regime that is inherent to fluid flow in microchannels, the geometry of the microdevice and the flow rates can be tuned to subject the cultured cells to well-defined, diffusion-independent concentration profiles. However, existing microfluidic gradient generators encounter hydrodynamic shear stresses that arise from the small characteristic dimensions of microfluidic channels. For most cultured cells, the maintenance of low levels of hydrodynamic shear is vital for the preservation of their integrity. To ensure a good laminar flow and gradient profile in the main

channel, the fluid that flows out from each small channel should have a symmetric flow rate pattern and different mixing ratios of two kinds of fluids.^{4–17} A symmetric flow rate pattern could be realized by a symmetric channel network. But this symmetric channel network will induce a non-linear gradient profile. It is very challenging to optimize the channel network which could realize both laminar flow and linear gradient profiles. Moreover, since the gradient generated by the laminar flow is not affected by the flow rate, Christmas tree designs also lack the function of dynamic control of the gradient profile. The initial fluid concentration from the inlet has to be changed if a different gradient profile needs to be studied. Since the laminar flow can only be maintained at low Reynolds numbers, the length of the gradient is also limited.

Another major approach is to leverage the diffusion to generate chemical gradients.^{21–34} The gradient generated by diffusion is vulnerable to convection flow. Thus the main issue with chemical gradient generators based on diffusion is the isolation of convection flow during the gradient generation procedure. For membrane-based diffusion chips,^{30–32,34} convection flows are physically isolated by thin membranes and only chemical molecules are allowed to diffuse through the membrane. For channel-based diffusion chips,^{28,33} convection flows are minimized by microchannels whose dimensions are much smaller than those of the main channels to maintain chemical gradients. Due to the isolation of convection flow, the gradients are mainly maintained at a low or even static flow rate with a minimal level of shear stress which is ideal for cell culture. On the other hand, the duration required to stabilize the gradient is relatively long because of the low flow rate. Once the gradient is formed, it is not easy to have a dynamic control of the gradient profile. Moreover, the gradient profile is mainly determined by the nature of diffusion; thus, linearity is not guaranteed. To

^a Department of Electrical and Computer Engineering and Singapore Institute for Neurotechnology (SINAPSE), National University of Singapore, Singapore 117576. E-mail: elelc@nus.edu.sg

^b Department of Biomedical Engineering and Singapore Institute for Neurotechnology (SINAPSE), National University of Singapore, 117575, Singapore

† Electronic supplementary information (ESI) available: 1) The fabrication process; 2) gradient profiles of both the accumulation method and dilution method with a flow rate of 500 nl min⁻¹ for inlet 1; 3) detailed process for cell culture and immobilization in the U-shaped main channel; 4) viability test of PC-9 cancer cells in a gradient from 0% to 90% generated by the accumulation method. See DOI: 10.1039/c4lc01451k

shorten the duration of stabilization of the gradient and enable an easier process for optimization and characterization, the length or area of the gradient is normally limited to the hundreds of micrometer scale.

Method

Here we present a novel gradient generation method based on convection-driven flow. This approach has many advantages over the methodologies developed so far since it can simultaneously satisfy the following: (1) the length of the gradient can be on the centimetre scale and the time to stabilize the gradient is short. (2) A linear gradient profile can be obtained which cannot be realized by Christmas tree designs and diffusion based designs. Thus the concentration gradient profiles can be relatively easily predicted. (3) The linear gradient profile can be tuned just by changing the flow rate which is not feasible in Christmas tree and diffusion based designs. (4) The device can work in both high flow rate regimes with large shear stress and low flow rate regimes with minimum shear stress.

Analysis and characterization

The principle of the gradient generator is shown in Scheme 1(a). An array of injection ports is connected to the main channel. The chemical solution is added to a flow of buffer solution in the main channel through injection ports. Due to the convection flow in the main channel, each segment of the main channel will have an accumulation of the chemical injected from the injection ports before this segment. Thus along the main channel, the concentration of the gradient will increase and a chemical gradient will be formed. The device used to realize this method is shown in Scheme 1(b). The device has a 3D structure with three layers. For the bottom layer, the U-shaped channel is the main channel used to generate the chemical gradient. The buffer solution is injected into inlet 1 of the main channel and extracted from outlet 1. Along the main channel, there is an

array of vertical injection ports in the middle layer. For the top layer, a channel network connects all vertical injection ports. The chemical used to generate the gradient is introduced to inlet 2 and injected into the main channel through the injection ports. This channel network looks similar to the channel network used in the Christmas tree design. But the structure and function of these two channel networks are different. In the Christmas tree design, two or more inlets are connected to the channel network and the main function of the channel network is to mix the fluids from the inlets in different ratios. In our design, the meandering channel network is connected to one inlet and designed to minimize the difference of the injection rate in each vertical injection port, achieving a linear gradient profile. Outlet 2 is designed to prevent any bubbles from remaining in the channel during the solution filling process at the beginning of the experiment. The detailed fabrication process and device characterization can be found in Fig. S1.†

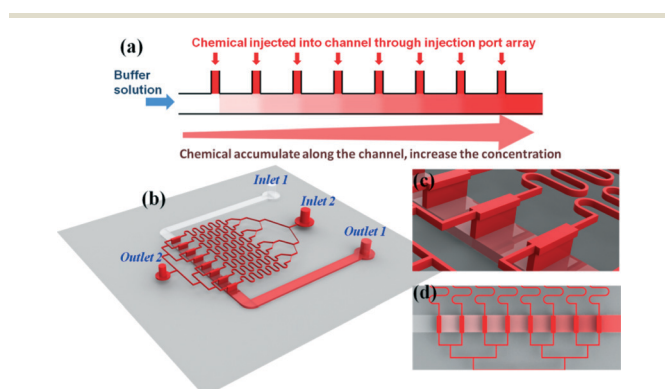
In this design, the length of the meandering channels is optimized to realize a linear gradient profile. However, the linear gradient profile can only cover the range from 0% to 50%. Thus a complementary method was developed to generate a gradient which can cover the range from 100% to 50%. Then a linear gradient covering a whole range from 0% to 100% can be generated by this gradient generator. Lastly, viability tests of PC-9 cancer cells were conducted to demonstrate the drug screening capability of this device.

To realize a linear gradient profile, the injection rate in each injection port at different positions in the main channel is expected to be identical. The flow rates in the injection ports are affected by the pressure applied to the connection part of the injection port and the main channel which varies with the position along the main channel. To minimize the difference of the flow rates in the injection ports, a discrete fluidic circuit model was built as shown in Fig. 1(a) to analyze the injection flow rates through the injection port array. The pressures applied to inlet 1 and inlet 2 are V_1 and V_2 , respectively. To simplify the design and optimization, the length of each meandering channel is identical. Thus the flow resistance of each meandering channel from inlet 2 to its injection port is the same, R_0 . The spacing of the injection port array is the same. So the flow resistance of the channel between two adjacent injection ports is the same, R_1 . The flow rate through each meandering channel is i_1 to i_n . Due to the flow through the U-shaped channel, there is a pressure drop along the channel. The pressure difference between two adjacent injection ports is from ΔV_1 to ΔV_n .

For the injection port n and $n + 1$, the flow rate is i_n and i_{n+1} . The flow rate difference is

$$\Delta i_n = i_{n+1} - i_n = \Delta \frac{V_n}{iR_0}$$

To ensure a linear gradient profile, the chemical concentration should have a linear increase along the U-shaped channel. Thus the flow rate through each injection port



Scheme 1 The working principle and structure of the chemical gradient generator; (a) working principle; (b) 3D illustration of the gradient generator; (c) detailed image of the vertical injection ports; (d) top view of the gradient maintained in the main channel.

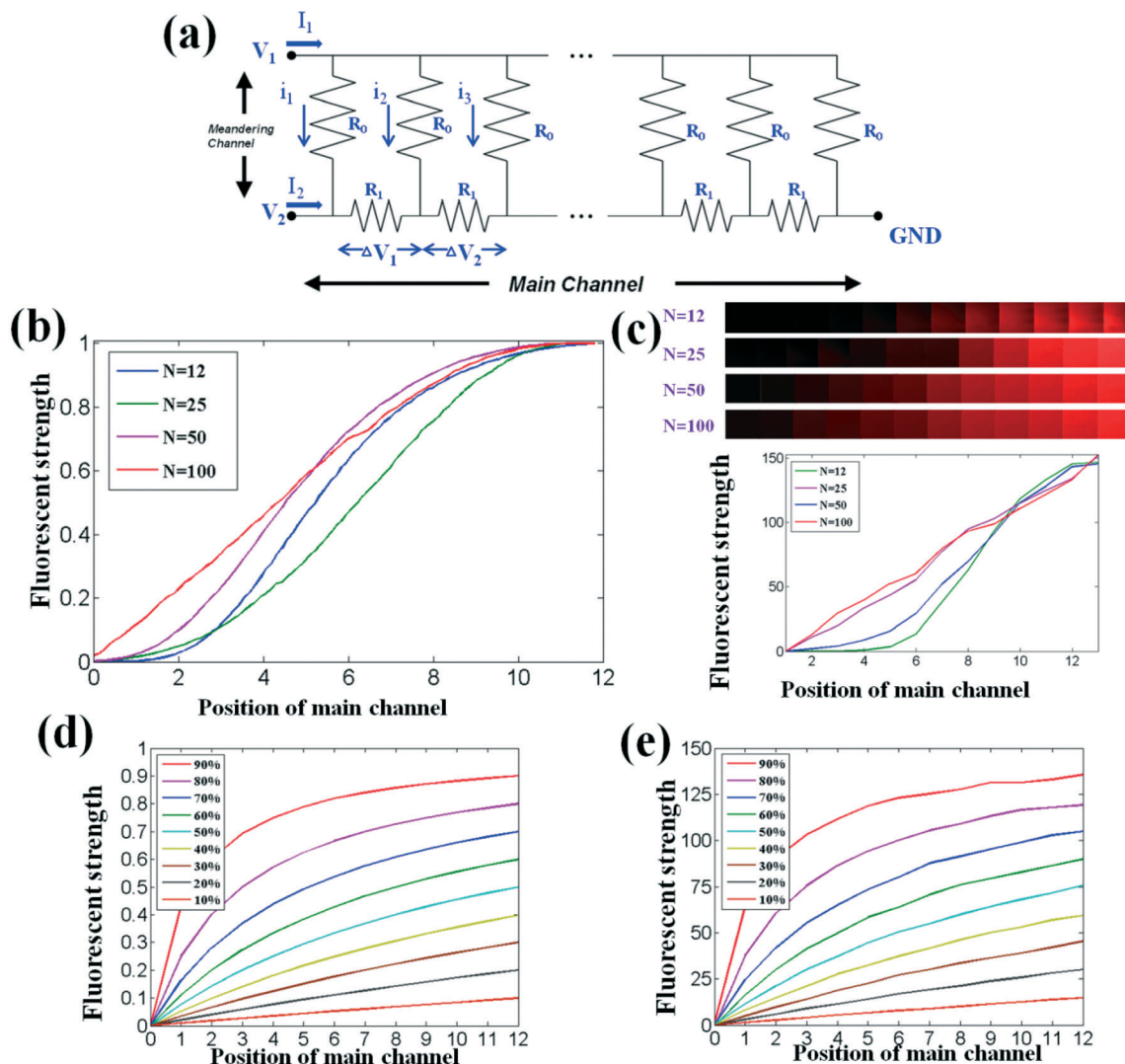


Fig. 1 (a) Discrete fluidic circuit model of the gradient generator; (b) simulation results of the gradient profiles by changing the length of the meandering channels; (c) experimental results of fluorescence images and gradient profiles by changing the length of the meandering channels; (d) the ideal curve of the gradient profiles when changing the final concentration at the end point; and (e) experimental results of the gradient profiles when changing the final concentration at the end point, where $N = 50$.

should be the same. But due to the ΔV induced by the flow resistance of the channel between two adjacent injection ports, Δi cannot be zero. However, when R_0 is close to infinity, Δi can be close to zero. Fig. 1(b) and (c) show representative chemical gradient profile results of mathematical modelling by COMSOL and experiments by using Rhodamine as the fluorescent dye. The number of injection ports is 12 and the length of the meandering channel ranges from 12 times ($N = 12$) to 100 times ($N = 100$) of the spacing between two adjacent injection ports. The ratio of the mass flow rates in inlet 1 and inlet 2 is 1:9 in mathematical modelling. So the final concentration is 10% at the end of the main channel. The flow rates to inlet 1 and inlet 2 were 100 nl min^{-1} and 11.1 nl min^{-1} , respectively, in the experiments. For the curve $N = 12$, injection ports close to inlet 1 have backflow from the main channel. Thus the concentration is close to zero for the first two ports in the curve. This is because the V_2 required to

drive the flow rate which is 1/9 of the flow rate injected from inlet 1 is much lower than V_1 when R_0 is very small. The flow rate i is negative for the injection ports close to inlet 1. As can be seen from the fluorescence image, the first part is dark. But the sum of the flow rates in all injection ports is constant. For the second half of the curve, the injection flow rates in the injection ports have a dramatic growth to balance the backflow. When the length of the meandering channels is increased, R_0 becomes larger thus the V_2 required to drive the flow also increases. The backflow disappears and the flow rate in each injection port tends to be identical. The profile of the gradient becomes linear when N is larger than 50 as can be seen in Fig. 1(b) and (c).

In general, when N is larger than 50, the difference of the flow rate in the injection port array could be neglected. The output of the injection ports could be considered identical. Under these ideal conditions, for a device with N injection

ports, the chemical concentration of segment n of the main channel is

$$C_n = \frac{\frac{n}{N}I_2}{I_1 + \frac{n}{N}I_2} \quad (1)$$

When I_2 is much smaller than I_1 , the $\frac{n}{N}I_2$ portion in the denominator can be neglected, which is the situation in Fig. 1(b) and (c) ($I_2 = \frac{1}{9}I_1$). The profile of the gradient should be

completely linear. But the linearity will deteriorate when I_2 increases. Fig. 1(d) shows the ideal curve of eqn (1) when the final concentration at the end of the channel ranges from 10% to 90% by increasing I_2 . As can be seen in Fig. 1(d), when the final concentration is not higher than 50%, the linearity is acceptable. The linearity increases with decreasing final concentration. Once the concentration is larger than

50%, meaning I_2 is higher than I_1 , the $\frac{n}{N}I_2$ portion in the denominator has a greater effect than I_1 . Thus the curve is not linear anymore. Fig. 1(e) shows the corresponding experimental results with the flow rate in inlet 1 equal to 100 nl min^{-1} and $N = 50$. For the results whose final concentration is not higher than 50%, the curve is linear. Once the concentration is higher than 50%, an obvious upper bending of the curve is observed, making the curve not linear. Therefore, by using this method to achieve a linear concentration profile, the final concentration cannot exceed 50%. But within the range from 0% to 50%, the linear gradient profile can have dynamic changes just by changing the flow rate ratio of inlet 1 and inlet 2.

Due to the linearity of the gradient, when the final concentration is known, which is determined by the flow rate ratio of inlet 1 and inlet 2, the concentration of each segment of the main channel can be predicted.

In general, the function of the channel network in our design is quite different from that of the channel network used in Christmas tree designs. The main purpose of the channel network is to ensure a linear profile rather than realize a solution mixture and laminar flow as in the Christmas tree design.

Cell viability test

To realize a chemical gradient with a range from 0% to 100%, a complementary method was developed. In the previous approach, the maximum linear range of the chemical gradient is 0% to 50%. The chemical solution is injected into the main channel through the injection ports and accumulated along the main channel. It is an accumulation approach. In this complementary method, we give the chemical solution to inlet 1 and the buffer solution to inlet 2. Then the linear range of the chemical gradient is from 100% to 50% which is the exact buffer solution gradient range in the previous method. The chemical solution in the main channel is diluted by the buffer solution from the injection ports. It is a dilution approach. Fig. 2(a) shows the experimental results of the accumulation approach and dilution approach. The flow rates in inlet 1 were kept at 100 nl min^{-1} , which is a low flow rate regime with low shear stress, for all experiments. All of the curves are linear as expected. We also conducted experiments with the flow rates in inlet 1 equal to 500 nl min^{-1} , which is a high flow rate regime with high shear stress. The results can be found in Fig. S2 of

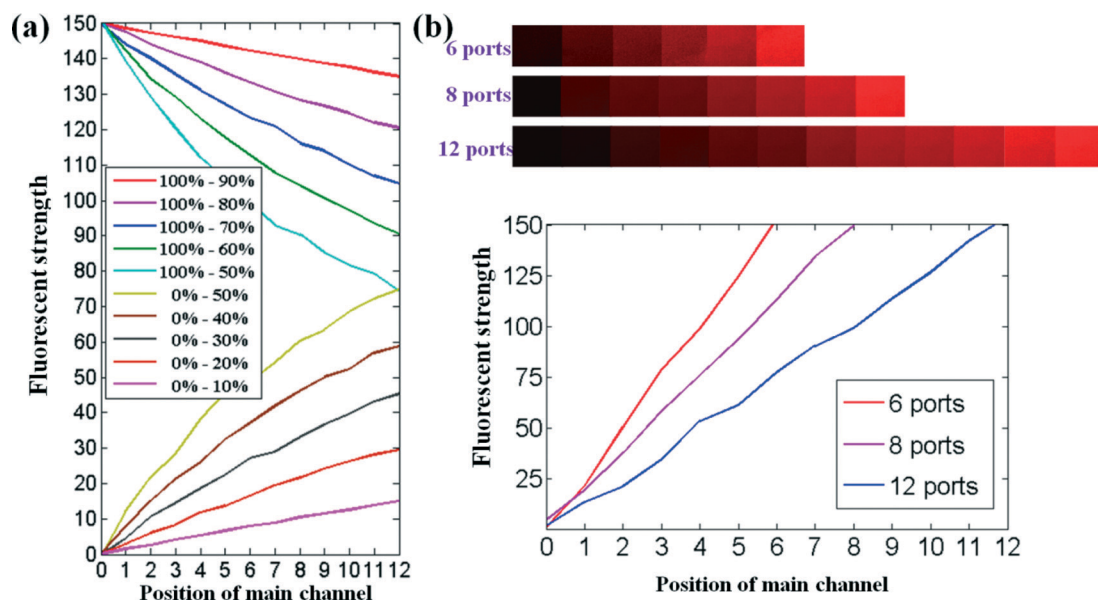


Fig. 2 (a) Experimental results of the gradient profiles using the accumulation method and dilution method. Gradient profiles starting from 100% were obtained by the dilution method. Gradient profiles starting from 0% were obtained by the accumulation method. (b) Experimental results of the gradient profiles from devices with different numbers of ports.

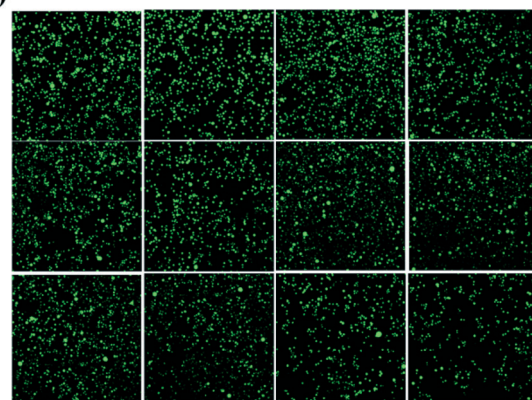
the ESI.† All of the curves are linear when the flow rates in inlet 1 and inlet 2 maintain the same ratio as in Fig. 2(a). The absolute values of flow rates do not have obvious effects on the gradient profile when the ratio of flow rates are kept the same.

The concentrations of different segments are discrete values in this method. Therefore, the resolution of the gradient is determined by the number of injection ports. More injection ports can result in a higher gradient resolution. Fig. 2(b) shows the experimental results obtained using 6, 8 and 12 ports with the same spacing between the ports. The final concentrations at the end points are 10%. $N = 50$ for all devices and the flow rates in inlet 1 are all 100 nl min^{-1} . The gradient profiles are all linear. The scale of the injection port array could be further extended to achieve a higher gradient resolution. However, the area needed to distribute the meandering channel will also have to be enlarged. Hence devices with more injection ports are not discussed here. Currently the spacing between two adjacent injection ports is $2000 \mu\text{m}$. Thus for a device with 12 injection ports, the length of the gradient is 2.4 centimetres. The length of the gradient could be further increased by increasing the number of injection ports. This centimetre scale linear gradient profile cannot be realized by either the Christmas tree designs or diffusion based designs.

To investigate the drug screening function of this device, the effect of doxycycline on the viability of PC-9 lung cancer cells was tested. A gradient of doxycycline solution was generated and maintained along the U-shaped main channel. The PC-9 cancer cells were immobilized onto the bottom substrate of the main channel. The detailed process for cell culture and immobilization in the U-shaped main channel can be found in the ESI.† The concentration of the doxycycline solution used in the experiment was 0.8 mg ml^{-1} . To realize a test range from 0% to 100%, the experiment was divided into two parts. For the first part, the accumulation method was used to generate a gradient from 0% to 50%. The doxycycline solution was injected into inlet 2 and culture medium was injected into inlet 1. For the second part, the dilution method was used to generate a gradient from 100% to 50%. The doxycycline solution was injected into inlet 1 and culture medium was injected into inlet 2. All of the flow rates in inlet 1 were 100 nl min^{-1} . The duration of the viability experiment was 2 hours. Calcein AM staining identified live cells along the main channel as shown in Fig. 3(a) and (b). The results of the accumulation method show a higher cell viability than the results of the dilution method. The viability of the cells decreased along the main channel using the accumulation method from 70% to around 32% as shown in Fig. 3(c).

In the dilution method, the viability of the cells increased along the main channel from 2% to around 25%. The final concentrations at the end points of the two methods were all 50%. But the two curves did not merge together at the end points because of the fluctuation of the results. As a comparison, the results for the gradient generated by

(a) Stained PC-9 cell by accumulation method from 0% to 50%



(b) Stained PC-9 cell by dilution method from 100% to 50%

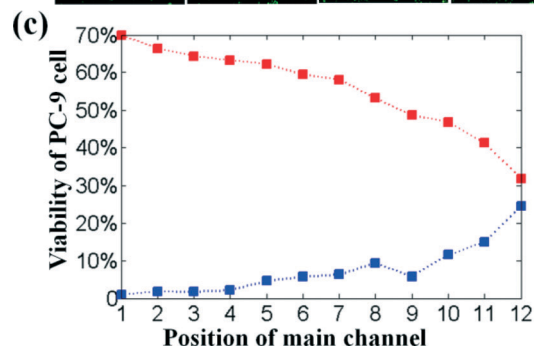
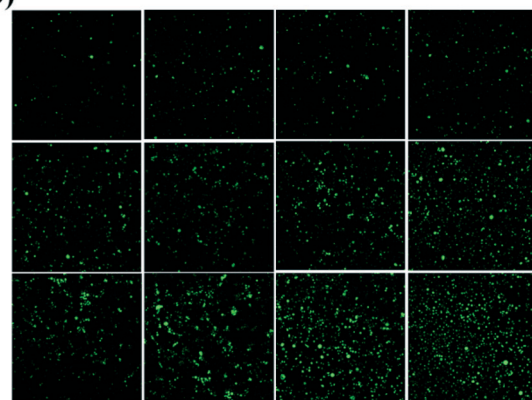


Fig. 3 PC-9 cell viability tests. (a) Calcein-AM stained PC-9 cancer cells from a concentration of 0% to 50% by the accumulation method; (b) calcein-AM stained PC-9 cancer cells from a concentration of 100% to 50% by the dilution method; and (c) viability of PC-9 cancer cells along the main channel in both the accumulation method and dilution method.

the accumulation method from 0% to 90% can be found in Fig. S3 in the ESI.† Due to the non-linear gradient profile, the results cannot characterize the viability of cells at all concentrations.

Conclusions

In summary, we designed and optimized a chemical gradient generator. The chemical gradient range could be tuned by changing the flow rates in the inlets. It could work in both low flow rate regimes and high flow rate regimes. The

resolution of the gradient can be improved by adding more injection ports. To achieve a linear gradient profile covering the range from 0% to 100%, two methods were developed. For the accumulation method, the maximum range was from 0% to 50%. For the dilution method, the maximum range was from 100% to 50%. Because of the high linearity, the concentrations of different segments can be predicted directly by knowing the position of the segment in the whole channel. This high linearity of the gradient profile cannot be achieved by other gradient generators. Since the convection flow is leveraged to generate the chemical gradient, the length of the gradient could be extended to the centimetre scale. The ability for drug screening was demonstrated by the cell viability experiments. In addition, the linear profile, the tunable gradient range and the ability to work with both low and high shear stresses make this device rather attractive for a variety of cell-based studies.

Notes and references

- 1 J. E. Phillips, K. L. Burns, J. M. Le Doux, R. E. Guldberg and A. J. Garcia, *Proc. Natl. Acad. Sci. U. S. A.*, 2008, **105**, 12170–12175.
- 2 F. Wang, *Cold Spring Harbor Perspect. Biol.*, 2009, **1**, a002980.
- 3 C. W. Chang, Y. J. Cheng, M. Tu, Y. H. Chen, C. C. Peng, W. H. Liao and Y. C. Tung, *Lab Chip*, 2014, **14**, 3762.
- 4 C. Kim, K. Kreppenhof, J. Kashef, D. Gradl, D. Herrmann, M. Schneider, R. Ahrens, A. Guber and D. Wedlich, *Lab Chip*, 2012, **12**, 5186–5194.
- 5 B. Y. Xu, S. W. Hu, G. S. Qian, J. J. Xu and H. Y. Chen, *Lab Chip*, 2013, **13**, 3714.
- 6 J. T. S. Fernandes, S. Tenreiro, A. Gameiro, V. Chu, T. F. Outeiro and J. P. Conde, *Lab Chip*, 2014, **14**, 3949–3957.
- 7 S. Ostrovidov, N. Annabi, A. Seidi, M. Ramalingam, F. Dehghani, H. Kaji and A. Khademhosseini, *Anal. Chem.*, 2012, **84**, 1302–1309.
- 8 D. Kim and C. L. Haynes, *Anal. Chem.*, 2012, **84**, 6070–6078.
- 9 Y. H. Jang, M. J. Hancock, S. B. Kim, S. Selimovic, W. Y. Sim, H. Bae and A. Khademhosseini, *Lab Chip*, 2011, **11**, 3277.
- 10 W. Siyan, Y. Feng, Z. Lichuan, W. Jiarui, W. Yingyan, J. Li, L. Bingcheng and W. Qi, *J. Pharm. Biomed. Anal.*, 2009, **49**, 806–810.
- 11 C. J. Wang, X. Li, B. Lin, S. Shim, G. Ming and A. Levchenko, *Lab Chip*, 2008, **8**, 227–237.
- 12 D. L. Englert, M. D. Manson and A. Jayaraman, *Appl. Environ. Microbiol.*, 2009, **75**, 4557.
- 13 D. L. Englert, M. D. Manson and A. Jayaraman, *Nat. Protoc.*, 2010, **5**, 864.
- 14 B. G. Ricart, B. John, D. Lee, C. A. Hunter and D. A. Hammett, *J. Immunol.*, 2011, **186**, 53–61.
- 15 B. G. Chung, L. A. Flanagan, S. W. Rhee, P. H. Schwartz, A. P. Lee, E. S. Monuki and N. L. Jeon, *Lab Chip*, 2005, **5**, 401–406.
- 16 G. Zheng, Y. Wang and J. Qin, *Anal. Bioanal. Chem.*, 2012, **404**, 3061–3069.
- 17 J. Ruan, L. Wang, M. Xu, D. Cui, X. Zhuo and D. Liu, *Mater. Sci. Eng., C*, 2009, **29**, 674–679.
- 18 A. Russom, D. Irimia and M. Toner, *Electrophoresis*, 2009, **30**, 2536–2543.
- 19 J. J. Vandersarl, A. M. Xu and N. A. Melosh, *Lab Chip*, 2011, **11**, 3057.
- 20 P. J. Hung, P. J. Lee, P. Sabounchi, R. Lin and L. P. Lee, *Biotechnol. Bioeng.*, 2005, 89.
- 21 M. E. Brett, R. DeFlorio, D. E. Stone and D. T. Eddington, *Lab Chip*, 2012, **12**, 3127–3134.
- 22 T. Frank and S. Tay, *Lab Chip*, 2013, **13**, 1273.
- 23 H. Wu, B. Huang and R. N. Zare, *J. Am. Chem. Soc.*, 2006, **128**, 4194–4195.
- 24 F. Piraino, G. C. Unal, M. J. Hancock, M. Rasponi and A. Khademhosseini, *Lab Chip*, 2012, **12**, 659.
- 25 J. He, Y. Du, J. L. Villa-Urbe, C. Hwang, D. Li and A. Khademhosseini, *Adv. Funct. Mater.*, 2010, **20**, 131–137.
- 26 Y. Du, J. Shim, M. Vidula, M. J. Hancock, E. Lo, B. G. Chung, J. T. Borenstein, M. Khabiry, D. M. Cropek and A. Khademhosseini, *Lab Chip*, 2009, **9**, 761–767.
- 27 M. Kim and T. Kim, *Anal. Chem.*, 2010, **82**, 9401–9409.
- 28 J. Atencia, G. A. Cooksey and L. E. Locascio, *Lab Chip*, 2012, **12**, 309.
- 29 J. Atencia, J. Morrow and L. E. Locascio, *Lab Chip*, 2009, **9**, 2707–2714.
- 30 U. Haessler, M. Pisano, M. Wu and M. A. Swartz, *Proc. Natl. Acad. Sci. U. S. A.*, 2011, **108**, 5614–5619.
- 31 U. Haessler, Y. Kalinin, M. A. Swartz and M. Wu, *Biomed. Microdevices*, 2009, **11**, 827–835.
- 32 S. Y. Cheng, S. Heilman, M. Wasserman, S. Archer, M. L. Shuler and M. Wu, *Lab Chip*, 2007, **7**, 763–769.
- 33 E. Cimetta, C. Cannizzaro, R. James, T. Biechele, R. T. Moon, N. Elvassore and G. Vunjak-Novakovic, *Lab Chip*, 2010, **10**, 3277–3283.
- 34 T. Ahmed, T. S. Shimizu and R. Stocker, *Nano Lett.*, 2010, **10**, 3379–3385.